Article

Cell

Gut Microbiota Orchestrates Energy Homeostasis during Cold

Graphical Abstract

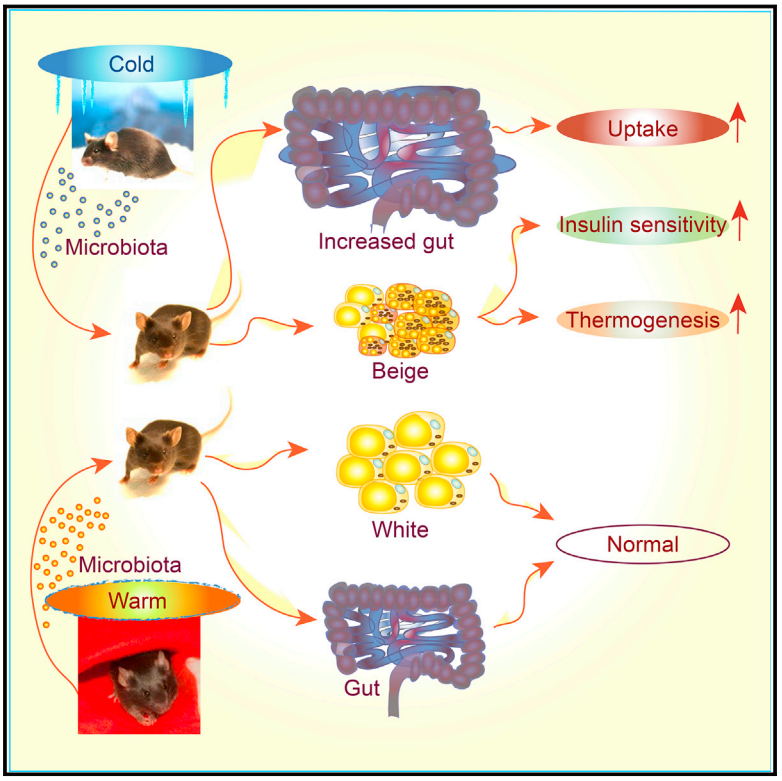

Authors

Claire Chevalier, Ozren Stojanović, Didier J. Colin, ..., Nicola Zamboni, Siegfried Hapfelmeier, Mirko Trajkovski

Correspondence

mirko.trajkovski@unige.ch

In Brief

Cold exposure markedly shifts the composition of the gut microbiota. This "cold microbiota" mediates remodeling of the fat and intestinal tissues, helping the host to withstand periods of high energy demand.

Highlights

- Cold exposure leads to marked changes in the gut microbiota composition
- Cold microbiota transplantation increases insulin sensitivity and WAT browning
- Cold exposure or cold transplantation increase the gut size and absorptive capacity
- Reconstitution of cold-suppressed *A. muciniphila* reverts the increased caloric uptake

Accession Numbers

GSE74228

Chevalier et al., 2015, Cell *163*, 1360–1374
December 3, 2015 ©2015 Elsevier Inc.
http://dx.doi.org/10.1016/j.cell.2015.11.004

Cell

Article

Gut Microbiota Orchestrates Energy Homeostasis during Cold

Claire Chevalier,[1,2,8] Ozren Stojanović,[1,2,8] Didier J. Colin,[3] Nicolas Suarez-Zamorano,[1,2] Valentina Tarallo,[1,2] Christelle Veyrat-Durebex,[1,2] Dorothée Rigo,[1,2] Salvatore Fabbiano,[1,2] Ana Stevanović,[1,2] Stefanie Hagemann,[4] Xavier Montet,[5] Yann Seimbille,[3] Nicola Zamboni,[6] Siegfried Hapfelmeier,[4] and Mirko Trajkovski[1,2,7,*]

[1]Department of Cell Physiology and Metabolism, Centre Médical Universitaire (CMU), Faculty of Medicine, University of Geneva, 1211 Geneva, Switzerland

[2]Diabetes Centre, Faculty of Medicine, University of Geneva, 1211 Geneva, Switzerland

[3]Centre for BioMedical Imaging (CIBM), Geneva University Hospitals, 1211 Geneva, Switzerland

[4]Institute for Infectious Diseases, University of Bern, 3010 Bern, Switzerland

[5]Division of Radiology, Geneva University Hospitals, 1211 Geneva, Switzerland

[6]Institute for Molecular Systems Biology, Swiss Federal Institute of Technology (ETH) Zurich, 8093 Zurich, Switzerland

[7]Division of Biosciences, Institute of Structural and Molecular Biology, University College London (UCL), London WC1E 6BT, UK

[8]Co-first author

*Correspondence: mirko.trajkovski@unige.ch

http://dx.doi.org/10.1016/j.cell.2015.11.004

SUMMARY

Microbial functions in the host physiology are a result of the microbiota-host co-evolution. We show that cold exposure leads to marked shift of the microbiota composition, referred to as cold microbiota. Transplantation of the cold microbiota to germ-free mice is sufficient to increase insulin sensitivity of the host and enable tolerance to cold partly by promoting the white fat browning, leading to increased energy expenditure and fat loss. During prolonged cold, however, the body weight loss is attenuated, caused by adaptive mechanisms maximizing caloric uptake and increasing intestinal, villi, and microvilli lengths. This increased absorptive surface is transferable with the cold microbiota, leading to altered intestinal gene expression promoting tissue remodeling and suppression of apoptosis—the effect diminished by co-transplanting the most cold-down-regulated strain *Akkermansia muciniphila* during the cold microbiota transfer. Our results demonstrate the microbiota as a key factor orchestrating the overall energy homeostasis during increased demand.

INTRODUCTION

Food intake, energy expenditure (EE), and body adiposity are homeostatically regulated, and malfunctions of this balance can cause obesity (Murphy and Bloom, 2006) (Farooqi and O'Rahilly, 2005). Mammalian white adipose tissue (WAT) is an important regulator of the whole body homeostasis that stores energy in form of triglycerides (TGs). The brown adipose tissue (BAT) catabolizes lipids to produce heat, function mediated by the tissue-specific uncoupling protein 1 (Ucp1) abundantly present in the BAT mitochondria. BAT differentiation can be induced by prolonged cold exposure and beta-adrenergic stimulation that leads to elevated intracellular cyclic AMP (Cannon and Nedergaard, 2004) (Young et al., 1984). The BAT is present at distinct anatomical sites, including the interscapular, perirenal, and axillary depots. Brown fat cells also emerge in subcutaneous WAT (SAT) (known as "beige" cells) in response to cold or exercise (Cousin et al., 1992) (Guerra et al., 2001), a process referred to as WAT browning. Loss of BAT function is linked to obesity and metabolic diseases (Lowell et al., 1993). Promotion of increased BAT development, on the other hand, increases EE without causing dysfunction in other tissues and is associated with a lean and healthy phenotype (Ghorbani et al., 1997; Guerra et al., 1998; Kopecky et al., 1995), suggesting the manipulation of the fat stores as an important therapeutic objective.

The gastrointestinal tract is the body's largest endocrine organ that releases a number of regulatory peptide hormones that influence many physiological processes (Badman and Flier, 2005). The intestinal epithelium undergoes rapid self-renewal fueled by multipotent Lgr5-expressing stem cells located in the crypts of Lieberkuhn and is terminated by apoptosis/exfoliation of terminally differentiated cells at the tips of small intestinal villi (Sato et al., 2009). At the apical surface, the epithelial cells have microvilli that further substantially increase the absorptive area and mediate the secretory functions. The intestinal microbiota co-develops with the host, and its composition is influenced by several physiological changes (Koren et al., 2012; Liou et al., 2013; Ridaura et al., 2013). The colonization starts immediately after birth and is initially defined by the type of delivery and early feeding. After 1 year of age, the intestinal microbiota is already shaped and stabilized but continues to be influenced by environmental factors including diet (Sekirov et al., 2010). A wide range of pathologies have been associated with alterations of the gut microbial composition (e.g., asthma, arthritis, autism, or obesity) (Sommer and Bäckhed, 2013). The intestinal microbiota can also influence the whole-body metabolism by affecting energy balance (Bäckhed et al., 2004) (Chou et al., 2008) (Turnbaugh et al., 2006) (Koren et al., 2012) (Ridaura et al., 2013). The mechanisms and the nature of the phenotypic and morphological changes that regulate the energy

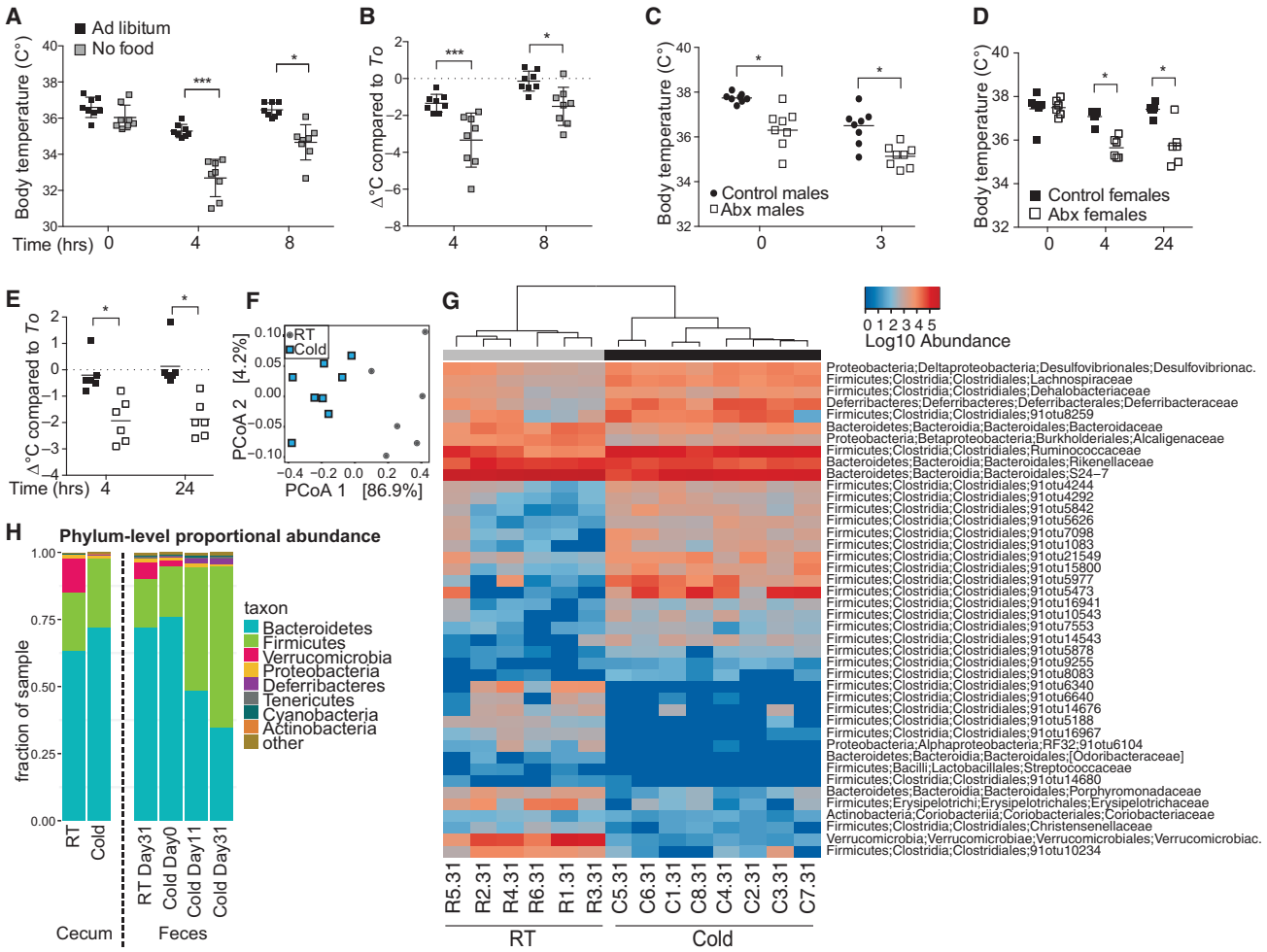

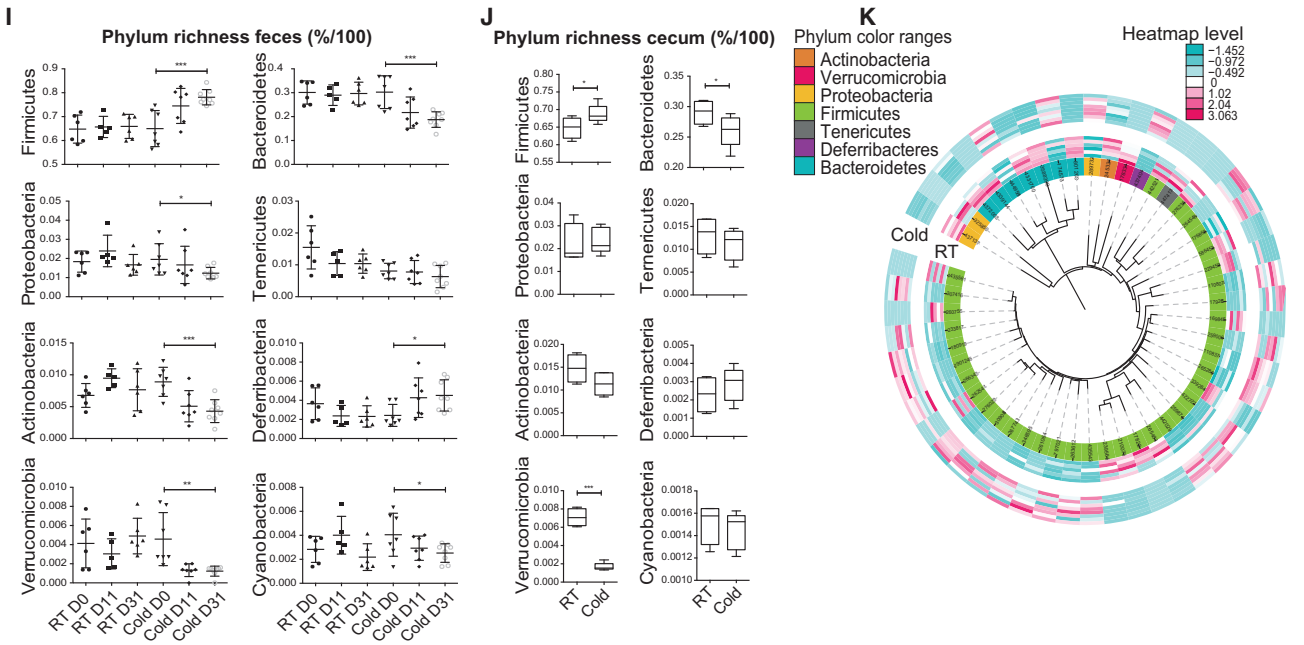

(legend on next page)

homeostasis of the new host following microbiota transplantation remain poorly understood. Here, we show that the microbiota remodeling is an important contributor of the beige fat induction during cold and a key factor that promotes energy uptake by increasing the intestinal absorptive area, thus orchestrating the overall energy homeostasis during increased energy demand.

RESULTS

Cold Exposure Changes the Gut Microbiota Composition

Short-term cold exposure for up to 10 days leads to increased EE relative to the energy uptake and suppresses BW and white fat mass gain (Figures S1A–S1F) (Wu et al., 2012, 2013). To investigate the importance of the acutely consumed food and caloric harvest during cold exposure, we restricted the food access during the initial 8 hr (hr) of cold exposure or depleted the intestinal microbiota using broad range antibiotics (Abx) administered in the drinking water. The higher fecal caloric content after complete microbiota depletion was confirmed using bomb calorimetry (Figure S1G) and was consistent with previous reports (El Kaoutari et al., 2013), suggesting lower energy harvest from the food. Restricting the food access during acute cold exposure led to decreased body temperature (Figures 1A and 1B) compared to ad libitum-fed control mice and to a marked drop in the blood glucose and BW at cold (Figures S1H–S1J). The decreased tolerance to cold and lowered blood glucose levels were also evident in the Abx-treated mice and the changes were relatively stable during short and long-term microbiota depletion up to 4 weeks of treatment (Figures 1C–1E and S1K–S1R), despite the stable food intake and slightly increased water consumption (Figures S1S and S1T). These data suggest that the energy harvest during acute cold contributes to maintaining the body temperature, and the intestinal microbiota is supporting this process.

We observed that over time, the overall fat loss was attenuated despite the stable food intake and EE (Figures S1A–S1F), suggesting compensatory mechanisms that enable increased caloric harvest from the consumed food. To investigate whether this prolonged cold exposure causes changes in the intestinal microbiota, we collected feces at days 0, 11, and 31 and cecum post-mortem of cold-exposed mice and room temperature (RT) controls. Profiling of the microbiota composition by 16S rRNA gene sequencing, followed by principal coordinates analysis (PCoA) based on weighted UniFrac distance, showed major alterations of the microbiota content both in cecum and feces samples of cold-exposed animals (Figures 1F, S2A, and S2B). As expected, Firmicutes was the richest phylum in all samples (on average 69.10%) (Figures 1I and 1J). Bacteroidetes was the most abundant phylum (on average 63.50%) in all samples except the cold-exposed day 31 samples (Figures S2C–S2E). We observed differences in operational taxonomic units (OTUs) abundance at phylum level in Bacteroidetes, Firmicutes, Verrucomicrobia, Deferribacteres, Cyanobacteria, and Actinobacteria, and differences in OTU numbers at phylum-level in all the above plus Deferribacteres based on factor summary bar chart. Individual species, or family-based hierarchical clustering using the average-neighbor method, confirmed the major shift of the microbiota composition and showed clustering of the samples from the cold-exposed versus the room temperature (RT) groups in both feces and cecum samples (Figures 1G, S2D, S2F, S3A, and S3B). Comparison of phylum level proportional abundance in feces showed shifts in proportions (Figures 1H and S2C), especially in the ratio Firmicutes/Bacteroidetes where Firmicutes abundance (from 18.6% in RT up to 60.5% under cold) increased over Bacteroidetes (from 72.6% in RT to 35.2% under cold). The Verrucomicrobia phylum was almost absent from both feces and cecum after the cold exposure (from 12.5% for the RT to 0.003% for the cold in cecum) (Figures 1H, S2C, and S2E). Interestingly, similar shifts, although less pronounced, are associated with genetic and high fat diet-induced obesity (Turnbaugh et al., 2006). The shifts in phylum abundance correlated with the richness of the species present in them. Firmicutes phylum increased its richness in feces up to 78.1% under cold exposure (compared to 65% in RT) and Bacteroidetes decreased it to 18.8% (compared to 29.7% in RT) (Figures 1I and 1J), without changing the overall bacterial diversity based on the Shannon diversity index (Figures S3C and S3D). From the 3,864 OTUs detected, using Welch t test done across the two groups of samples using the abundance metrics, 252 OTUs (within 44 families) were significantly different ($p < 0.05$). Of the selected families, there were mixed responses in Firmicutes, Proteobacteria, and Bacteroidetes, however, those within Actinobacteria,

Figure 1. Cold Exposure Changes the Gut Microbiota Composition

(A) Rectal body temperature (BT) of food restricted or ad libitum-fed C57Bl6J mice after 4 and 8 hr (hr) of cold exposure (n = 8 per group).

(B) Change in BT compared to initial as in (A).

(C) Rectal BT after 3 hr of cold exposure of male mice treated or not treated with antibiotics (n = 8 per group).

(D) Rectal BT after 4 hr and 24 hr of cold exposure in antibiotics-treated or control female mice (n = 6 per group).

(E) Change in BT compared to initial as in (D).

(F) Principal coordinates analysis (PCoA) based on weighted UniFrac analysis of OTUs. Each symbol represents a single sample of feces after 31 days of cold-exposed (n = 8) or RT controls (n = 6 per group).

(G) Hierarchical clustering diagram using the average-neighbor (HC-AN) method comparing feces of 31 days cold-exposed mice (n = 8) and their RT controls (n = 6). Associated heatmap shows the relative abundance of representative OTUs selected for $p < 0.05$, obtained with a Welch t test comparison of the two groups and then grouped into families. One representative OTU with the greatest difference between the two group means from each family is selected for inclusion in the heatmap diagram. OTUs are shown as: Phylum, Class, Order, Family, Genus, and Species. R, RT; C, cold-exposed.

(H) Comparison of phylum-level proportional abundance of cecum and feces of up to 31 days cold-exposed or RT control mice.

(I and J) Richness represented as the proportions of OTUs classified at the phylum rank. (I) Feces. (J) Cecum. In (H)–(J) n = 5 + 6 (cecum) or 6 + 8 (feces).

(K) Heatmap tree comparing selected OTUs abundance from feces of RT controls (n = 6, inner rings) and 31 days cold-exposed mice (n = 8, outer rings) and their phylogenic relationships. The OTUs representative of differentially abundant families are selected as described in (H).

See also Figures S1, S2, and S3.

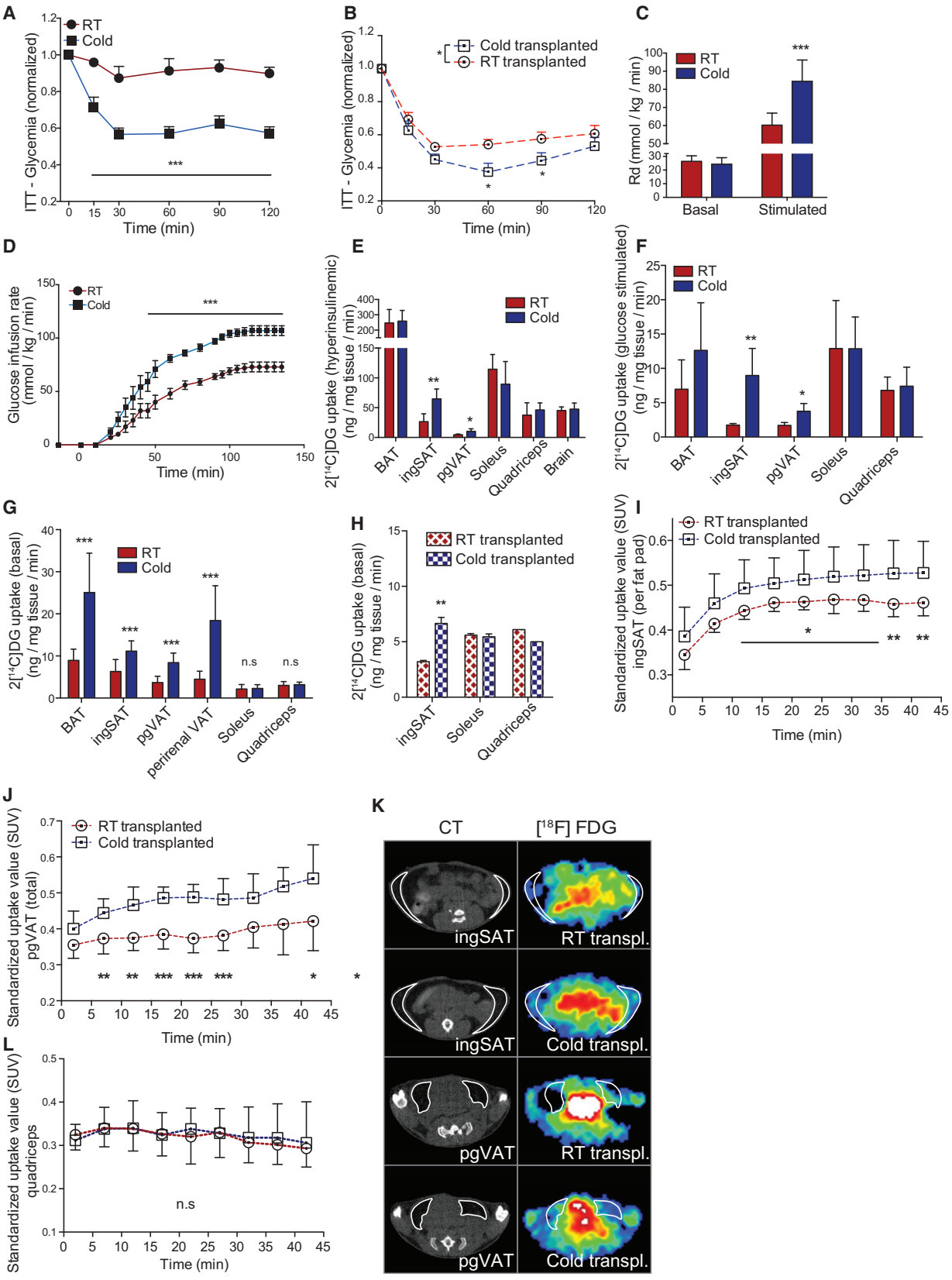

(legend on next page)

Verrucomicrobia, and Tenericutes were less abundant in the cold samples, while RT samples were less abundant in Deferribacteres (Figure 1K). When looking at the most significantly changed OTUs using analysis of variance, *Akkermansia muciniphila* and S24-7 family were among the top nine most shifted bacteria (Figures S3G and S3H). Verrucomicrobia phylum was represented by eight different OTUs, all part of the same species: *Akkermansia muciniphila*, which we found highly decreased with cold exposure (Figures S3E and S3F). The changes in the major bacterial phyla were confirmed by qPCR in the sequenced, as well as in independent sets of SPF and conventional animals (Figures S3I–S3L). Together, these results demonstrate a major shift in lower gut microbiota in response to cold exposure.

Cold Microbiota Transplantation Increases Insulin Sensitivity

To investigate the importance of the microbiota changes during cold, we transplanted the microbiota from 30 days cold-exposed or control RT mice to germ-free (GF) mice by co-habitation and again confirmed the shifts in the donors and the recipient mice (Figures S3K and S3L). As expected, cold exposure of donor mice led to a marked increase in the insulin sensitivity (Figure 2A). Strikingly, cold microbiota transplanted mice also showed increased sensitivity to insulin (Figure 2B), suggesting that cold microbiota alone is sufficient to transfer part of this phenotype. The increased insulin sensitivity was further investigated using hyperinsulinemic-euglycemic clamp in awake and unrestrained mice. Cold mice showed a marked increase in the glucose infusion rates (GIR) needed to maintain the clamped glucose levels and an increase in the stimulated glucose disappearance (Rd) levels (Figures 2C, 2D, and S4A). To investigate the peripheral glucose uptake, we co-administered 2-[^{14}C]deoxyglucose (2[^{14}C]DG) during the clamp. While no changes were observed in the glucose uptake from interscapular BAT (iBAT), brain, soleus, or quadriceps muscle, there was a large increase in the uptake from inguinal subcutaneous and perigonadal (epididymal in males) visceral depots of the WAT (ingSAT and pgVAT, respectively) (Figure 2E). These observations were further corroborated in glucose-stimulated and basal conditions (Figures 2F and 2G), which in addition showed increased glucose uptake in iBAT. Interestingly, the cold microbiota transferred the fat-specific glucose disposal phenotype to the transplanted mice as measured by 2[^{14}C]DG uptake (Figure 2H) and by positron emission tomography-computed tomography (microPET-CT). Specifically, both ingSAT and pgVAT, but not quadriceps muscle, showed increased [^{18}F]fluorodeoxyglucose ([^{18}F]FDG) uptake in the cold-transplanted mice (Figures 2I–2K) and had decreased ingSAT and pgVAT volumes and weights (Figures 3A–3F and S4B). Hounsfield unit (HU) analysis of the microCT scans revealed that cold microbiota-transplanted mice had higher ingSAT and pgVAT density compared to the controls (Figures 3G and 3H). Together, these data suggest that the cold microbiota contributes to the increased insulin sensitivity observed during cold exposure and leads to decreased total fat coupled with increased fat density.

Cold Microbiota Promotes Browning, Energy Expenditure, and Cold Tolerance

To investigate whether the higher density and the decreased fat amount (Figures 3A–3H) are originating from the differences in the adipocyte volume, we measured the adipocyte size distribution using high content imaging. Cold-transplanted mice had increased number of small and decreased number of large adipocytes in the ingSAT and pgVAT depots (Figures 3I–3L). The adipose depots excised from the cold-transplanted animals were darker in appearance. All these phenotypic events are characteristic features of mature beige adipocytes. Therefore, we investigated whether cold microbiota could affect the browning of the white fat depots and found that cold-transplanted mice had marked increase in the brown fat-specific markers in the ingSAT, and surprisingly, also in the pgVAT depots (Figures 3M and 3O). The increased browning of ingSAT was consistent with the increased Ucp1-positive cells in the cold-transplanted mice (Figure 3N). There was a tendency bordering significance toward increased brown fat marker expression in the interscapular BAT (iBAT) depots of the cold-transplanted mice, albeit at smaller scale compared to ingSAT and pgVAT (Figure 3P). Together, these data suggest that cold microbiota alone can be sufficient to induce beige/brown fat formation primarily in the ingSAT and pgVAT, and to a smaller magnitude, in the iBAT depots. The increased browning was consistent with the enhanced resting EE (REE) of the cold-transplanted mice (Figure 3Q), suggesting increased energy dissipation. To further investigate its functional relevance, we exposed the cold-transplanted mice to acute cold and monitored the internal body temperature, as well as ventrally or dorsally, indicative of the temperature emitted from ingSAT or iBAT depots. The rectal temperature measurements showed that the RT-transplanted mice had decreased body temperature following 4 hr of cold exposure, but only a mild temperature drop was detected in the cold-transplanted mice (Figures 4A and 4B). Accordingly, the infrared imaging and quantification of the different regions

Figure 2. Cold Microbiota Transplantation Increases Insulin Sensitivity and WAT Glucose Uptake

(A and B) Intraperitoneal insulin tolerance test (ITT) in RT and 25 days cold-exposed mice (A), or RT- and cold microbiota-transplanted mice (B) relative to initial blood glucose, (n = 8 per group).

(C–E) Euglycemic-hyperinsulinemic clamp of awake mice as in (A). Rate of disappearance of ^{3}H-D-glucose (C). GIR time course during the hyperinsulinemic clamp (D). 2[^{14}C]DG uptake in various tissues (E) (n = 6 + 6).

(F) 2[^{14}C]DG tracer uptake in tissues 45 min after IP tracer and glucose (2 g/kg BW) administration in mice as in (A) (n = 6 per group).

(G and H) 2[^{14}C]DG uptake in tissues 30 min after administration under basal conditions in anesthetized RT (n = 9) and cold (n = 10) (G); or RT- and cold-transplanted mice (n = 3) (H).

(I, J, and L) Positron emission tomography-computer tomography (microPET-CT) measurement of [^{18}F]FDG uptake in ingSAT (I), pgVAT (J), or quadriceps muscle (L) in basal conditions of RT- and cold-transplanted mice as in (B) (n = 6 per group).

(K) Transversal [^{18}F]FDG PET-CT images of ingSAT and pgVAT of mice as in (I) and (J).

See also Figure S4.

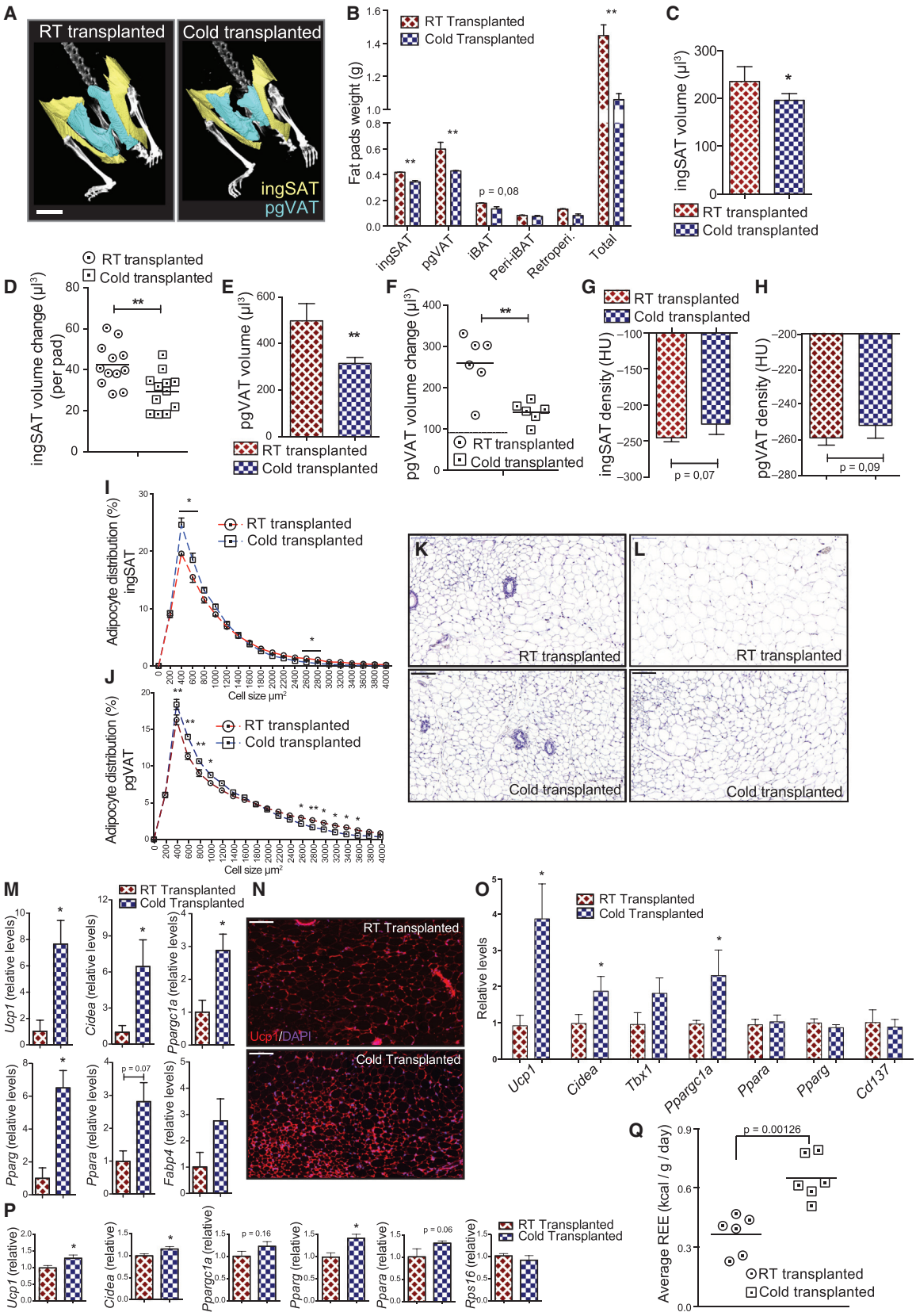

(legend on next page)

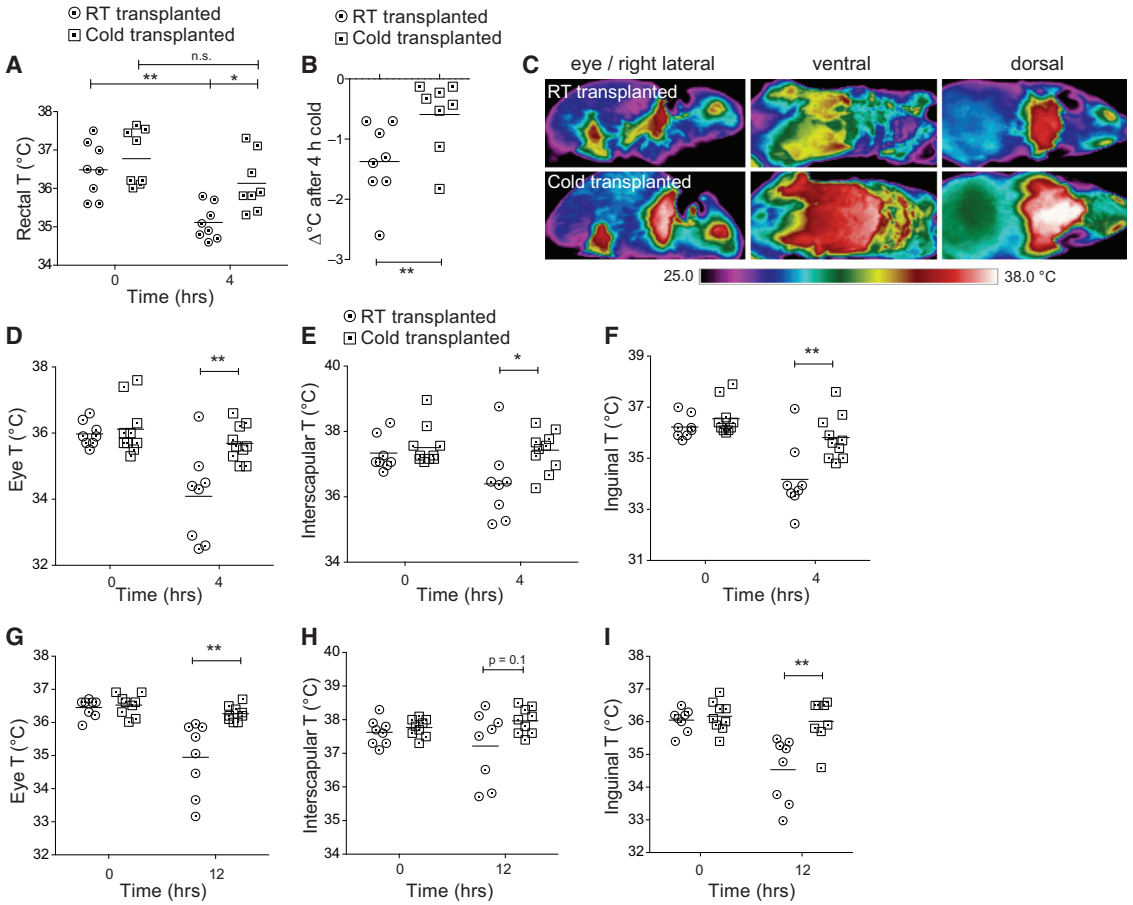

Figure 4. Cold Microbiota Prevents Hypothermia

(A and B) Rectal temperature (A) or temperature change (B) of RT- or cold-transplanted mice before or after 4 hr of cold exposure (n = 8 per group).

(C) Infrared images of representative RT- or cold-transplanted mice after 4 hr cold exposure.

(D–F) Infrared temperature readings from eye (D), ventral (E), or dorsal (F) region of mice as in (C) before or after 4 hr of cold exposure.

(G–I) Infrared temperature readings from eye (G), ventral (H), or dorsal (I) region of mice as in (C) before or after 12 hr of cold exposure.

(Figure 4C) demonstrated that cold microbiota-transplanted mice are fully resistant to cold stress as shown by the eye temperature measurements, representative of the internal body temperature (Figures 4D and 4G). Analysis of the dorsal and ventral infrared images showed that the inguinal and the interscapular regions contribute to the overall tolerance to cold. Specifically, while the differences in dorsal temperatures were transient between the groups (Figures 4E and 4H), the maximal ventral heat differences remained constant also after 12 hr of cold exposure (Figures 4F and 4I). These data suggest a mechanistic explanation for the increased insulin sensitivity and demonstrate that the cold microbiota alone is sufficient to induce tolerance to cold, increased EE, and lower fat content, and this effect is partially mediated by the browning of the white fat depots.

Figure 3. Cold Microbiota Promotes Browning of WAT

(A) 3D reconstitution of the ingSAT and pgVAT of cold- and RT-transplanted mice 21 days after transplantation using the CT scans. Scale bar, 5 mm.

(B) Weight of fat pads of cold- or RT-transplanted mice after 5.5 weeks (n = 6 per group).

(C–H) IngSAT or pgVAT volumes (C and E), or densities (G and H) of mice as in (A). Change in each fat pad volume (D and F) (n = 12 per group, except [E] and [F] where n = 6 per group) of same mice scanned at day 3 and day 21 after transplantation.

(I and J) Cell size profiling of adipocytes from ingSAT (I), or pgVAT (J) of RT- or cold-transplanted mice 21 days after transplantation. The values show % from the total number of analyzed cells. Bars show mean of the pooled corresponding fractions from each animal ± SEM (n = 6 for each panel).

(K and L) H&E staining on paraffin sections from ingSAT (K) or pgVAT (L) of RT- or cold-transplanted mice.

(M, O, and P) Relative mRNA expression in ingSAT (M), pgVAT (O), or iBAT (P) of RT- or cold-transplanted mice (n = 6 per group), quantified by real-time PCR and normalized to the house keeping beta-2-microglobulin (B2M).

(N) Immunohistochemistry of Ucp1 and DAPI on paraffin sections from ingSAT in RT- or cold-transplanted mice as in (K).

(Q) Resting energy expenditure (REE) in RT- or cold-transplanted mice, measured between day 3 and day 21 after bacterial colonization (n = 6 per group).

Scale bars in (K), (L), and (N), 100 μm.

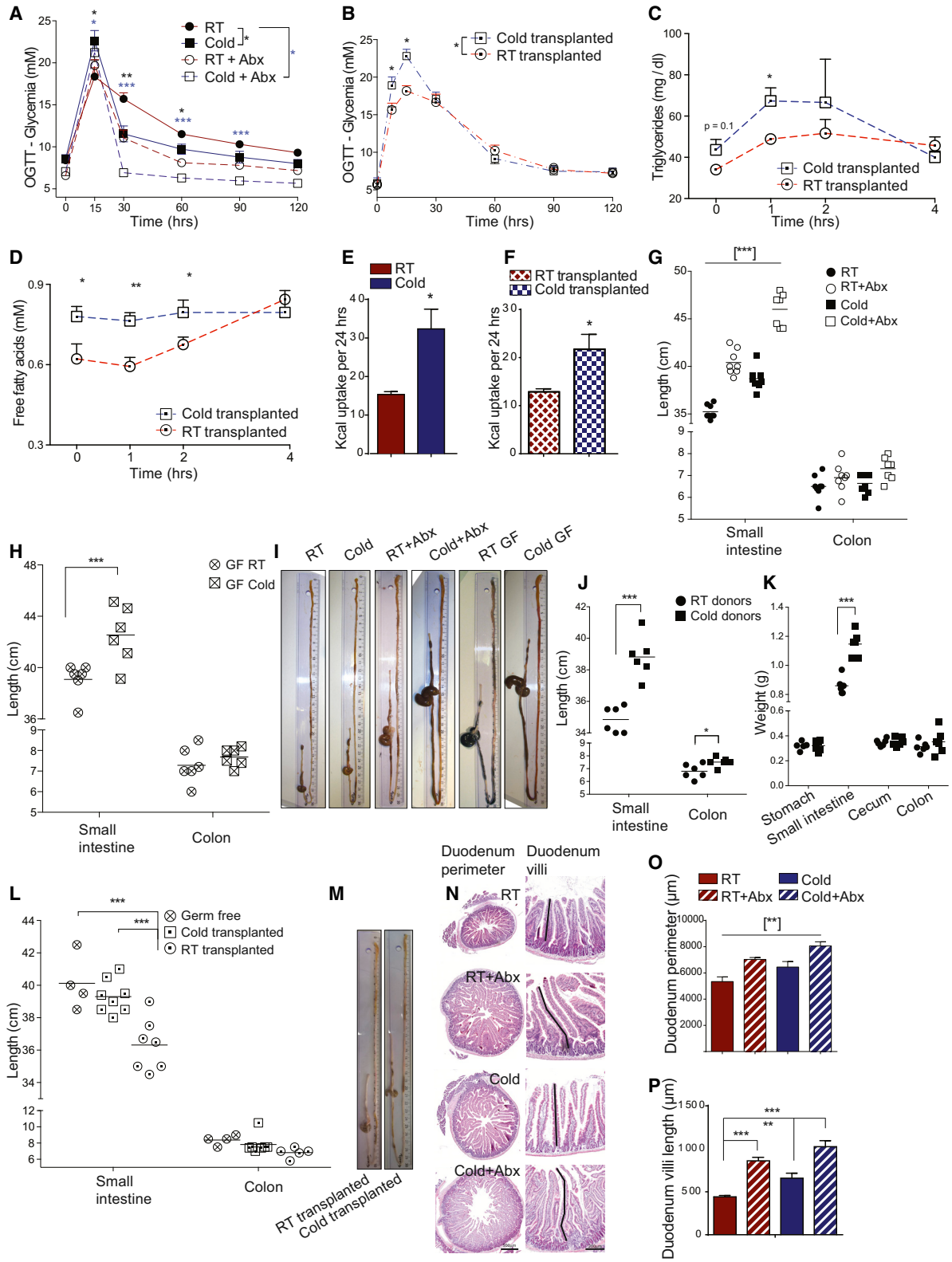

Figure 5. Cold-Exposed and Cold Microbiota-Transplanted Mice Show Increased Intestinal Length and Caloric Uptake

(A and B) Oral glucose tolerance test (OGTT) of cold-exposed mice with or without Abx treatment (A), or RT- and cold microbiota-transplanted mice 16 days after transplantation (B) (n = 8 per group).

(legend continued on next page)

Cold-Exposed and Cold Microbiota-Transplanted Mice Have Increased Intestinal Absorptive Surface

Next, we monitored short-chain fatty acids (SCFAs), volatile compounds, and organic acids associated with gut flora activity using mass spectrometry (Tables S1 and S2). In lipid cecal extracts, butyrate, the primary energy source in colon and the most abundant SCFA (Ferreyra et al., 2014), was markedly decreased in antibiotic-treated mice and, accordingly, increased upon gut flora transplantation (Table S2). Similarly, succinate, a frequent product of primary fermenters that is utilized by butyrogenic bacteria (Wichmann et al., 2013), was decreased in the absence of gut flora. We observed increase of propionate, butyrate, lactate, and succinate in cold-transplanted mice (Table S2). These results could indicate increased fermentation activity of cold over RT microbiota, associated with increased energy harvest.

As mentioned, during long-term cold exposure and after the initial weight loss, the BW stabilizes despite the constantly increased EE rates and heat production, suggesting increased nutrient absorption from the relatively stable food intake. Oral glucose tolerance tests (OGTT) in cold-exposed mice with or without microbiota depletion showed an elevated glucose peak following glucose gavage compared to RT controls (Figures 5A and S4C–S4G) after 15 min, but also faster clearance, consistent with the increased insulin sensitivity (Figure S4H). Interestingly, no differences were observed in the initial glucose peak when glucose was administered intraperitoneally (Figure S4I). This suggests that orally administered glucose is rapidly taken up in cold-exposed mice and in microbiota-depleted mice. The rapid glucose uptake was observed also in the cold-transplanted mice, which showed increased glucose peaks 7.5 and 15 min after glucose gavage (Figure 5B) and no changes in the insulin release compared to the RT-transplanted (Figure S4J). This was consistent with increased triglyceride uptake and non-esterified fatty acid levels in the cold-transplanted mice (Figures 5C and 5D), suggesting increased total energy harvest levels following oral gavage in the cold-transplanted mice. To confirm that cold exposure leads to increase in the calorie uptake, we measured the fecal caloric content using bomb calorimetry and calculated the total energy uptake. Cold-exposed mice showed increased caloric uptake, and this was phenocopied in the cold-transplanted mice (Figures 5E and 5F). These data suggested increased intestinal absorptive capacity following cold exposure, which is transferable by the microbiota transplantation. We therefore looked at the intestine in more detail and observed a marked increase in the lengths and weights of the small intestine in the cold-exposed mice as early as 9 days after initiation of cold exposure (Figures S5A–S5C), persisting up to 30 days of cold (Figures 5G and S5D). Microbiota depletion also led to increased intestinal length and weight, however, the changes in this case were more pronounced after 30 days of Abx treatment and were consistent with the increased intestinal length in the GF mice (Figures 5G–5I and S5D). Cold exposure of the Abx-treated and GF mice led to dramatic increases of their intestinal lengths amounting to almost 35% and weights of over 150% compared to the RT controls, demonstrating remarkable plasticity of the small intestinal absorptive tissue in response to the increased energy demand (Figures 5G–5I, S5D, and S5E). The rest of the tissues, such as the colon, stomach, iBAT, or quadriceps muscle did not show obvious morphological changes (Figures S5D–S5G), except the decreased WAT levels described above. The increased intestinal length was still present 3 weeks after the end of the cold exposure in the donor mice that were used to transplant the GF mice (Figure 5J). Strikingly, cold microbiota-transplanted mice also showed a marked increase in the intestinal lengths and weights compared to the RT-transplanted controls, suggesting that the microbiota contributed to this phenotype (Figures 5L, 5M, and S5K). To further investigate the changes in the intestinal morphology, we measured the intestinal perimeter and villus length and found that both were increased in the cold mice and were further enlarged in the cold-exposed Abx-treated mice (Figures 5N–5P). This characteristic, however, was not transferred by the microbiota transplantation, consistent with the proportional increase in the intestinal lengths and weights in the transplanted mice, compared to the donors in which the ratio weight versus length increased by 1.8-fold.

To investigate the intestinal morphological changes, we quantified the relative contribution of the different cell types composing it—stem cells and Paneth cells in the bottom of the crypt and enterocytes, goblet cells, and enteroendocrine cells along the villi. In our models, the number of the enteroendocrine cells was increased in the cold-exposed and cold-exposed Abx-treated mice, but also in the cold-transplanted mice, proportional to the overall increase in the average cell number (Figures S6A–S6E). There was an antibiotics-dependent effect in the number of goblet cells, which were increased upon microbiota depletion, but no changes were observed in the cold-transplanted mice (Figures S6F–S6H, S6L, and S6M).

(C and D) Plasma triglycerides (C) and free fatty acids (D) during oral fat tolerance test in RT- or cold microbiota-transplanted mice as in (B) (n = 6 per group).
(E and F) Total caloric uptake during 24 hr of cold- or RT-exposed (E), or RT-transplanted (F) mice (n = 8 per group). Mice were kept two per cage. Each cage was considered as one pooled sample (n = 4). Data in (E) and (F) show mean ± SEM.
(G and H) Small intestine and colon lengths of cold-exposed mice with or without Abx treatment (n = 8 per group) (G) or cold-exposed and RT-kept GF mice (n = 6 per group) (H).
(I) Representative images of cecum, small intestine, and colon of mice as in (E)–(H).
(J) Small intestine and colon lengths of 30 days cold-exposed or RT-kept donor mice used for microbiota-transplantation, 23 days after start of cohabitation at RT (n = 6 per group).
(K) Stomach, small intestine, cecum, and colon weights of donor mice as in (J).
(L) Small intestine and colon lengths of RT- or cold microbiota-transplanted mice as in (B) (n = 8 per group), 21 days after transplantation, and GF controls (n = 4).
(M) Representative images of cecum, small intestine, and colon of mice as in (L).
(N–P) H&E staining of duodenum of cold-exposed mice with or without Abx treatment (N) and morphometric quantifications of duodenal perimeter (O) and villi length (P) (n = 8 per group in triplicates, data show mean ± SEM).
See also Figures S5 and S6.

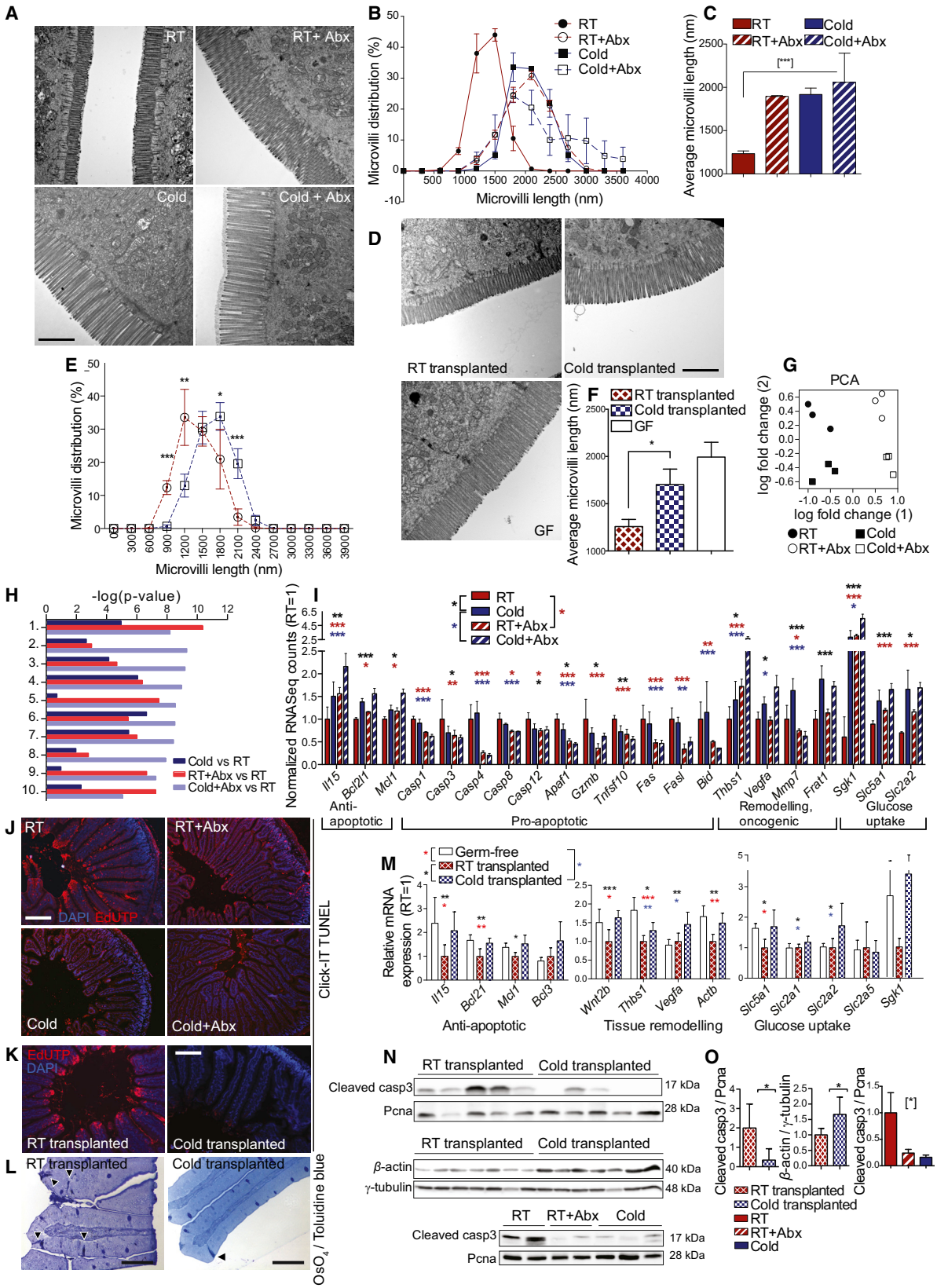

(legend on next page)

Olfm4 is a highly specific and robust marker for Lgr5 positive stem cells. Quantification of the Olfm4+ cells showed increment only in the intestine of cold-exposed Abx-treated mice, consistent with their most pronouncedly enlarged intestine (Figures S6I–S6K). These data suggest that cold exposure leads to a number of changes in the intestinal composition, which in the case of the enteroendocrine cells, are in part transferable by cold microbiota transplantation.

Microvilli form the brush border on the apical epithelial surface of the small intestine, and a single enterocyte can have as many as 1,000 microvilli, each one formed by cross-linked actin bundles. They increase the surface area of the absorptive cell ~25-fold. Using quantitative electron microscopy (EM), we found that the microvilli length is substantially increased in the cold-exposed, as well as in microbiota-depleted mice (Figures 6A–6C), thus further largely increasing the intestinal surface area. Strikingly, these differences were also transferred in the cold microbiota-transplanted mice, which showed increased microvilli lengths (Figures 6D–6F). Together, these results demonstrate that during increased energy demand, specifically cold exposure, there is a dramatic increase in the intestinal absorptive surface area due to the increased intestinal, villi, and microvilli lengths, and cold microbiota transfer alone can be sufficient to induce these changes.

Reduced Apoptosis Underlies the Increased Intestinal Surface

To uncover the mechanisms of the microbiota-epithelium cross-talk responsible for the observed gut phenotype, we deep sequenced the transcriptome from proximal jejunum of RT, RT+Abx, Cold, and Cold+Abx mice. The expression profiles markedly differed between the groups (Figure 6G), and unbiased pathway enrichment analysis revealed changes in pathways involved in cytoskeletal remodeling, tissue growth, WNT signaling, apoptosis, and immune response common for mice with increased intestinal surface (Cold, RT+Abx, and Cold+Abx), when compared to RT mice (Figures 6H, 6I, and S6N). Anti-microbial response and TNF signaling, which promote apoptosis and cell shedding, and are activated by bacteria through NF-κB and TLR pathways (Hausmann, 2010; Spehlmann and Eckmann, 2009), were strongly suppressed in all microbiota-depleted mice (Figure S6N). Indeed, apoptosis and anti-apoptotic interleukin-15 signaling (Obermeier et al., 2006) were among the top-regulated pathways in the mice with increased intestinal surface (Figures 6H, 6I, and S6N). Using the TUNEL assay, we observed that compared to the RT mice, the apoptosis was markedly reduced in the villi of all other groups (Figure 6J). This phenotype was transferred in the cold-transplanted animals, which retained the anti-apoptotic phenotype of the GF and Abx-treated mice (Figures 6K–6O). Conversely, RT-transplanted mice acquired increased apoptosis, exhibited reduction of the anti-apoptotic *Il15*, *Bcl2l1* (coding isoform Bcl2-XL), and *Mcl1* expression (Pelletier et al., 2002) and showed increased caspase 3 activation (Figures 6M–6O). Concomitantly, the mice with increased intestinal surface had augmented vascularization and tissue remodeling gene expression and showed marked increase in the main apical (Sglt1, gene *Slc5a1*) and basolateral (Glut2, *Slc2a2*) glucose transporters (Figures 6I and 6M). Together, these data suggest a mechanistic explanation of the increased intestinal surface area and glucose permeability, which can be transferred by the cold microbiota transplantation.

Cold Microbiota Increases Intestinal Absorption in an *Akkermansia-muciniphila*-Sensitive Manner

To finally demonstrate that the increased intestinal surface corresponds to enhanced absorptive capacity of the intestine, we did ex vivo experiments in isolated segments from the middle to proximal jejunum of the microbiota-transplanted mice. Mucosal to serosal D[1-^{14}C] glucose (D[^{14}C]G) apparent diffusion coefficient was higher in cold-transplanted mice (Figure 7A), suggesting increased intestinal glucose absorption. This was consistent with the increased D[^{14}C]G present in intestinal tissue after 1 hr of transport and lower residual D[^{14}C]G levels in the lumen (Figures 7B and 7C). Cold microbiota mice also had prolonged intestinal transit time, proportional to the increase in the intestinal length of the corresponding animals (Figure 7D). Since the increased intestinal surface area was also present in the microbiota-depleted mice, we assumed that absence of certain bacterial strains, rather than increased abundance, could be responsible for the observed intestinal phenotype following the cold microbiota

Figure 6. Presence and Composition of Microbiota Determine Length of Microvilli on Brush Border of Small Intestine

(A and D) Electron micrographs of jejunal enterocyte microvilli of cold-exposed mice with or without Abx treatment (A), or GF, RT-, and cold microbiota-transplanted mice 19 days after transplantation (D). Scale bars, 2 μm.

(B and E) Morphometric quantification of microvilli length distribution in (B) as in (A) and (E) as in (D).

(C and F) Average microvilli lengths of mice as in (A) and (D), respectively.

(G) Principal component analysis (PCoA) of gene expression data in proximal jejunum of mice as in (A).

(H) Top commonly regulated pathways (MetaCore pathway enrichment) in RT, RT+Abx, Cold, and Cold+Abx differential gene expression comparisons. Legend: 1: immune response, TNF-R2 signaling; 2: main growth factor signaling cascades; 3: IGF family signaling in colorectal cancer; 4: c-Kit ligand signaling during hemopoiesis; 5: apoptosis and survival; 6: GM-CSF signaling; 7: TGF, WNT, and cytoskeletal remodeling; 8: signal transduction, AKT signaling; 9: cell adhesion, chemokines and adhesion; and 10: IL-15 signaling via JAK-STAT cascade.

(I and M) Relative mRNA expression in proximal jejunum of mice as in (A), or GF, or RT- and cold microbiota-transplanted GF (M) quantified by RNA seq (I) or real-time PCR (M) and normalized to the average expression of the housekeeping *Rplp0* (36b4) and *Rps16* (GF are n = 4; rest are n = 8 per group). Significance in (I) was calculated using general linear model with negative binomial distribution.

(J and K) Terminal deoxynucleotidyl transferase (dUTP) nick end labeling (TUNEL) assay for apoptotic cells double labeled with DAPI of proximal jejunum paraffin sections of mice as in (A) or (D). Scale bars, 200 μm.

(L) Semi-fine 1-μm thick EM sections of proximal jejunum stained with toluidine blue displaying apoptotic cells in dark blue (marked with arrowheads) of mice as in (D). Round, goblet cells. Scale bar, 20 μm.

(N and O) Western blotting of lysates from proximal jejunum of mice as in (D) and (A) and respective quantifications (O) normalized to loading controls.

See also Figure S6.

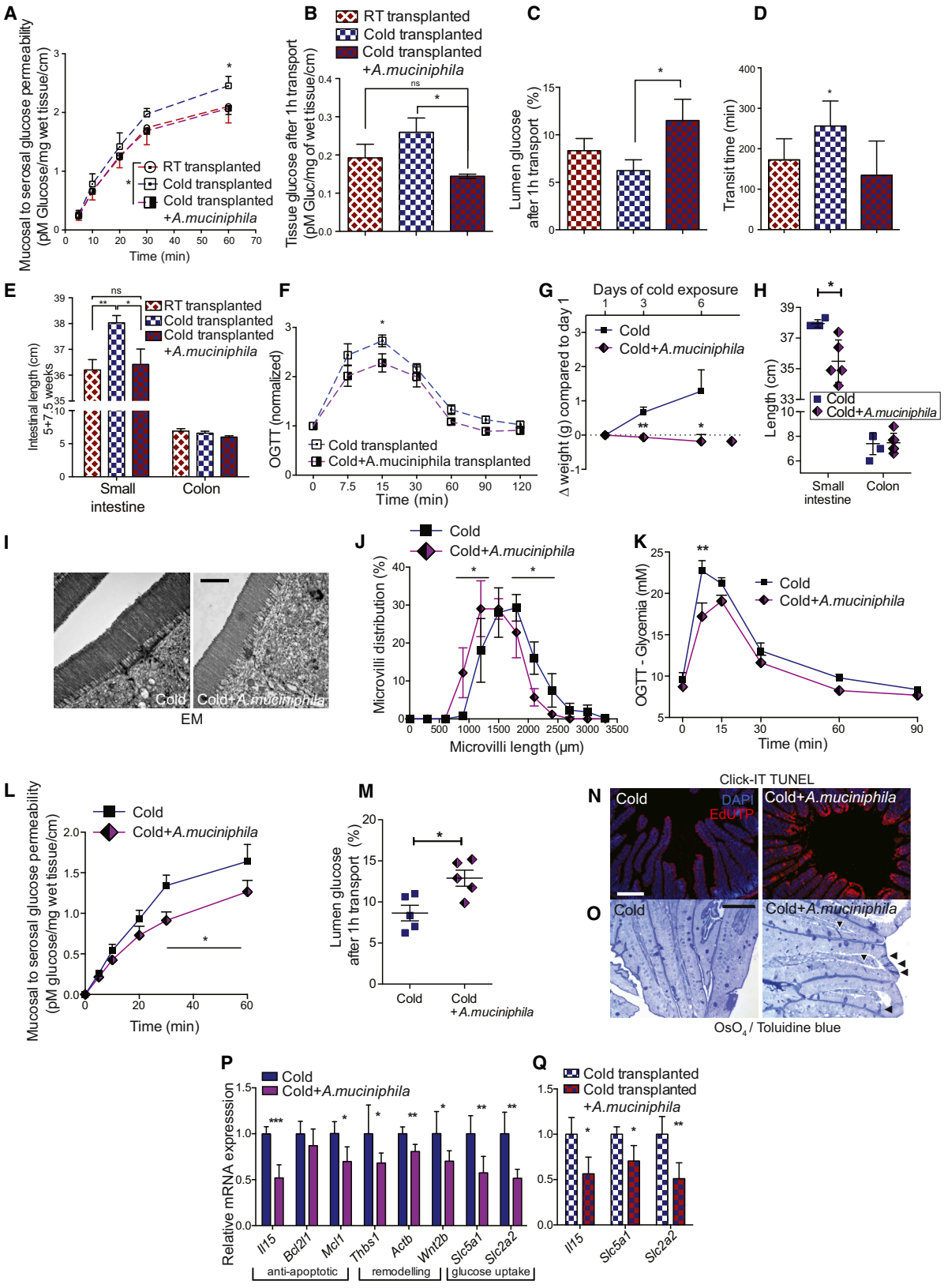

(legend on next page)

transplantation. *Akkermansia muciniphila* (*A. muciniphila*) is a Gram-negative bacterium that commonly constitutes 3%–5% of the gut microbial community. *A. muciniphila* within the mucus layer is implicated in the control of host mucus turnover (Belzer and de Vos, 2012), which improves gut barrier function and is linked to obesity (Everard et al., 2013). Since *A. muciniphila* is the most abundant species of the Verrucomicrobia, the most negatively affected phylum in response to cold exposure, we investigated whether this strain alone could revert part of the transplanted phenotype. Co-transplantation of *A. muciniphila* fully prevented the cold microbiota transferable increase of the intestinal glucose absorption (Figures 7A–7C) and decreased the intestinal transit time (Figure 7D). Moreover, the increased intestinal length caused by cold microbiota transplantation was fully reverted in the cold microbiota + *A. muciniphila*-transplanted animals (Figures 7E and S7A). These results were consistent with the OGTT, which showed a limited increase in the glucose peak 15 min after the gavage (Figure 7F) and no differences in the insulin levels between the groups (Figure S7B). Neither differences were observed in the tolerance to insulin and cold, nor in the expression of the beige fat markers (Figures S7C–S7J), together suggesting that *A. muciniphila* does not negatively affect the browning or the sensitivity to insulin. Interestingly, *A. muciniphila* colonization reverted the changes in the Bacteroidetes/Firmicutes ratio in the cold-transplanted mice (Figures S7K and S7L). Therefore, we investigated the importance of the rest of the bacterial consortium by mono-colonizing GF mice with *A. muciniphila* and observed no differences in the intestinal length and duodenum perimeter, while there was a small decrease of the microvilli length bordering significance (Figures S7M–S7P), suggesting that *A. muciniphila* is necessary, but not sufficient to revert the intestinal lengthening. In contrast, daily gavage of *A. muciniphila* to cold-exposed mice decreased their BW and fat mass gain and shortened their intestine and microvilli after 7 days of cold exposure. The Bacteroidetes/Firmicutes abundance was not yet affected by the cold exposure at this time interval, showing that changes in their ratio is not a prerequisite for the intestinal remodeling, and change in *A. muciniphila* precedes the remodeling of these major phyla (Figures 7G–7J and S7Q–S7T). *A. muciniphila* re-colonization during the cold exposure decreased the OGTT peak and prevented the cold-induced increase in the intestinal absorptive capacity (Figures 7K–7M and S7U). Accordingly, re-colonizing *A. muciniphila* reverted the cold-induced decrease in the apoptosis levels and reduced the expression of the key tissue remodeling, anti-apoptotic, and glucose uptake genes during cold (Figures 7N–7Q). Combined, these results underscore that the cold exposure-induced decrease of *A. muciniphila* enables increasing the intestinal absorptive surface by altering several key regulatory pathways, and co-transfer of this strain together with the cold microbiota, or during the cold exposure, is sufficient to prevent the adaptive increase in the intestinal absorptive functions that maximize the caloric uptake during cold.

DISCUSSION

During evolution, mammals developed a number of adaptive responses to energy scarcity. Microbial diversity of the human gut is the result of co-evolution between microbial communities and their hosts. We assumed that this co-evolution favored maximizing uptake of calories from the consumed food during periods of increased energy demand, such as cold exposure. Indeed, cold exposure led to dramatic changes of the microbiota composition, increasing Firmicutes versus Bacteroidetes ratios and almost completely depleting the Verrucomicrobia phylum. We found that these changes favored enhanced energy extraction during cold. Interestingly, in part this is rendered possible by an adaptive mechanism of the host that increases the overall intestinal absorptive surface, due to a marked elongation of the total intestinal, villi, and microvilli lengths. When transplanted to GF-recipient mice, the cold microbiota alone was sufficient to promote this increased intestinal absorptive surface area by lengthening the gut and the epithelial microvilli. Similar changes in the gut morphology were observed in microbiota-depleted mice, which is also a condition of negative energy balance, suggesting that the increase in the intestinal absorptive surface is a general adaptive mechanism promoting caloric uptake when food is available.

Figure 7. Cold Microbiota Increases Intestinal Absorption Due to Absence of *A. muciniphila*

(A–C) Ex vivo measurements of glucose transport in jejunal segments excised from RT-, cold-, and cold+ *A. muciniphila*-transplanted mice (n = 5 per group); with mucosal to serosal glucose permeability (A), radioactive glucose tracer in tissue (B), and in the lumen (C) of jejunum segment after 1 hr of transport.

(D) Intestinal transit time of RT-, cold-, and cold+ *A. muciniphila*-transplanted mice as in (A) (n = 6 per group).

(E) Intestinal length in mice transplanted with RT (n = 9), cold (n = 10), and cold+ *A. muciniphila* (n = 6) microbiota 6 weeks after transplantation.

(F) OGTT in cold- (n = 10) and cold+ *A. muciniphila* (n = 6)-transplanted male mice as in (A).

(G) Body weight change compared to day 0 of 7-week-old mice, exposed to cold for 7 days and gavaged daily with fresh *A. muciniphila* or vehicle (PBS) (n = 5 per group).

(H) Intestinal length of mice as in (G).

(I) Electron micrographs of jejunal enterocyte microvilli of mice as in (G) Scale bar, 2 μm.

(J) Morphometric quantification of microvilli length distribution of the EM images as shown in (I) (n = 5 per group).

(K) OGTT of mice as in (G) 6 days after start of treatment.

(L and M) Ex vivo measurements of glucose transport in jejunal segments excised from mice as in (G) (n = 5 per group); with mucosal to serosal glucose permeability (L), radioactive glucose tracer in tissue after 1 hr of transport (M).

(N) TUNEL assay for apoptotic cells double-labeled with DAPI of proximal jejunum paraffin sections of mice as in (G). Scale bar, 200 μm.

(O) Semi-fine 1-μm thick EM sections of proximal jejunum stained with toluidine blue showing apoptotic cells in dark blue (marked with arrowheads). Round, goblet cells. Scale bar, 20 μm.

(P and Q) Relative mRNA expression in proximal jejunum of mice as in (G) or (A), (P) or (Q), respectively, quantified by real-time PCR and normalized to the average expression of the house keeping *Rplp0* (36b4) and *Rps16*.

See also Figure S7.

In absence of microbiota, epithelial survival was promoted by removal of pro-apoptosis signals, upregulation of growth factor cascades, and increase in glucose transport. Colonization by different gut consortia interfered with these changes to different extents, either keeping most of them (cold microbiota) or restoring them to normal levels (RT or cold+ *A. muciniphila* colonization). Cold exposure of the microbiota-depleted mice, however, further increased the intestinal length, suggesting that additional factors also contribute to this process. The observed increased intestinal absorptive capacity in absence of *A. muciniphila* could give additional explanation to its function in obesity, where absence of this bacterium enables increased uptake in surrounding of excess energy despite the constant intestinal length. This is consistent with our ex vivo data that show decreased glucose permeability in presence of *A. muciniphila* in isolated equal (2 cm long) jejunal segments and suggests that absence of this bacterium is necessary, but may not be sufficient to increase the intestinal length. Here, we demonstrate that also in conditions of negative energy balance and lean and healthy phenotype, *A. muciniphila* absence enables increased caloric uptake. All this suggests that this bacterium may act as an energy sensor that is abundant during caloric deficiency and is low when the energy is in excess, as a co-evolutionary mechanism enabling the energy uptake when available. Indeed, *A. muciniphila* is elevated in undernourished mice (Preidis et al., 2015) as a typical example of energy scarcity, while it is absent during cold where food intake is strongly increased. Maintaining the increased gut length and absorptive surface is energy-requiring. To ensure that the intestinal lengthening pays off, this process would need to depend on whether the energy needed to maintain the increased intestinal surface is justified in promoting overall increase in the energy balance, which is not the case in conditions of low food abundance. Seen in this context, *A. muciniphila* is a unique example of host microbial mutualism regulating the energy homeostasis and enabling positive energy balance.

In addition, our data demonstrate that the cold microbiota alone is sufficient to induce tolerance to cold, increased EE, as well as lower fat content, and this effect is at least, in part, mediated by browning of the white fat depots. This provides mechanistic explanation for the increased insulin sensitivity following cold microbiota transplantation, since increased browning protects against obesity and insulin resistance (Ghorbani et al., 1997; Guerra et al., 1998; Kopecky et al., 1995). *A. muciniphila* on the other hand could not explain the browning following microbiota transplantation, suggesting that additional changes in the intestinal microbiota are mediating this. Thus, discriminating and narrowing down the exact bacterial species affecting this would be an interesting area of future study. Fecal microbiota transplantation was reported almost 50 years ago (Eiseman et al., 1958) and has re-gained interest as a treatment option for several pathologies (Ley et al., 2006; Kelly, 2013; Khoruts, 2014). In the context of the increased obesity prevalence and energy unbalance, our study showing microbiota changes that promote weight loss and energy dissipation, imply microbiota as a key player mediating the tight control of the energy homeostasis with large therapeutic potential.

EXPERIMENTAL PROCEDURES

Animals

All C57Bl/6J (wild-type [WT]) mice (Charles River) were kept in a specific pathogen-free facility (SPF) in 12-hr day/night cycles, unless otherwise specified. Germ-free (GF) mice were on C57Bl/6 background from the germ-free facility of the University of Bern and were kept in sterile conditions until sacrificed, unless otherwise stated. All mice were kept two per cage. Fresh antibiotics (100 μg/ml neomycin, 50 μg/ml streptomycin, 100 U/ml penicillin, 50 μg/ml vancomycin, 100 μg/ml metronidazole, 1 mg/ml bacitracin, 125 μg/ml ciprofloxacin, 100 μg/ml ceftazidime, and 170 μg/ml gentamycin [Sigma; Alkaloid]) were administered in the drinking water and changed once a week as described (Grivennikov et al., 2012). Cold exposures were done at 6°C in a light- and humidity-controlled climatic chamber (TSE) in SPF conditions using individually ventilated cages. Acclimatized animals were allocated to groups based on their body weights and blood glucose levels to ensure equal starting points. Microbiota transplantations were done by co-housing GF mice with cold-exposed donors at RT for 10 days or by gavage of 20 mg fresh feces resuspended in 400 μl sterile anaerobic PBS. Mice were treated with *A. muciniphila* by oral gavage at a dose of 2×10^8 cells/0.2 ml suspended in sterile anaerobic PBS as previously described (Everard et al., 2013). All experiments were started in 7- to 8-week-old male mice unless otherwise specified. All animal experiments were approved by the Swiss Federal and Geneva Cantonal authorities for animal experimentation.

Statistical Analysis

Unless otherwise specified in the figure legends, significance was calculated using non-paired two-tailed Student's t test (*$p \leq 0.05$, **$p \leq 0.01$, ***$p \leq 0.001$). Brackets in Figures 5G, 5O, and S5D indicate comparisons of all pairs in the dataset. All values in the figure panels show mean ± SD. All experiments were done at least three times, and the representative experiment is shown. Sample sizes and animal numbers were chosen based on power calculations of 0.8.

ACCESSION NUMBERS

The accession number for the sequencing data reported in this paper is NCBI GEO: GSE74228.

SUPPLEMENTAL INFORMATION

Supplemental Information includes Supplemental Experimental Procedures, seven figures, and three tables and can be found with this article online at http://dx.doi.org/10.1016/j.cell.2015.11.004.

AUTHOR CONTRIBUTIONS

C.C., O.S., N.S.Z., V.T., D.R., S.F., and A.S designed and performed experiments and analyzed data. D.J.C., Y.S., and X.M. did PET-CT and CT measurements, N.Z. measured metabolites. S.H. and S.H. provided GF mice and participated in mono-colonizations. M.T. designed the work, performed experiments, analyzed data, prepared the figures, and wrote the manuscript with input from all co-authors.

ACKNOWLEDGMENTS

We thank Maria Gustafsson Trajkovska, Claes Wollheim, and Roberto Coppari for discussions and critical reading; Jean-Baptiste Cavin and André Bado for sharing expertise in intestinal loop; Christian Darimont for help with bomb calorimetry; Abdessalam Cherkaoui and Jacques Schrenzel for the use of anaerobic incubator; (ERC-2013-StG-281904) to S.H. for partial support of the gnotobiotic research; Mirosava Ilievska for providing antibiotics; Mario Kreutzfeldt and Doron Merkler for help with histology quantifications; and Gabriel Waksman for support. The research leading to these results has received funding from the European Research Council under the European Union's Seventh Framework Programme (FP/2007-2013)/ERC grant agreement

336607 (ERC-2013-StG-336607); the Louis-Jeantet Foundation; Fondation pour Recherches Médicales; Novartis Foundation (14B053); and the Swiss National Science Foundation (SNSF) Professorship (PP00P3_144886) to M.T.

Received: May 20, 2015
Revised: September 11, 2015
Accepted: October 28, 2015
Published: December 3, 2015

REFERENCES

Bäckhed, F., Ding, H., Wang, T., Hooper, L.V., Koh, G.Y., Nagy, A., Semenkovich, C.F., and Gordon, J.I. (2004). The gut microbiota as an environmental factor that regulates fat storage. Proc. Natl. Acad. Sci. USA *101*, 15718–15723.

Badman, M.K., and Flier, J.S. (2005). The gut and energy balance: visceral allies in the obesity wars. Science *307*, 1909–1914.

Belzer, C., and de Vos, W.M. (2012). Microbes inside–from diversity to function: the case of Akkermansia. ISME J. *6*, 1449–1458.

Cannon, B., and Nedergaard, J. (2004). Brown adipose tissue: function and physiological significance. Physiol. Rev. *84*, 277–359.

Chou, C.J., Membrez, M., and Blancher, F. (2008). Gut decontamination with norfloxacin and ampicillin enhances insulin sensitivity in mice. Nestle Nutr. Workshop Ser. Pediatr. Program. *62*, 127–137, discussion 137–140.

Cousin, B., Cinti, S., Morroni, M., Raimbault, S., Ricquier, D., Pénicaud, L., and Casteilla, L. (1992). Occurrence of brown adipocytes in rat white adipose tissue: molecular and morphological characterization. J. Cell Sci. *103*, 931–942.

Eiseman, B., Silen, W., Bascom, G.S., and Kauvar, A.J. (1958). Fecal enema as an adjunct in the treatment of pseudomembranous enterocolitis. Surgery *44*, 854–859.

El Kaoutari, A., Armougom, F., Gordon, J.I., Raoult, D., and Henrissat, B. (2013). The abundance and variety of carbohydrate-active enzymes in the human gut microbiota. Nat. Rev. Microbiol. *11*, 497–504.

Everard, A., Belzer, C., Geurts, L., Ouwerkerk, J.P., Druart, C., Bindels, L.B., Guiot, Y., Derrien, M., Muccioli, G.G., Delzenne, N.M., et al. (2013). Cross-talk between Akkermansia muciniphila and intestinal epithelium controls diet-induced obesity. Proc. Natl. Acad. Sci. USA *110*, 9066–9071.

Farooqi, I.S., and O'Rahilly, S. (2005). Monogenic obesity in humans. Annu. Rev. Med. *56*, 443–458.

Ferreyra, J.A., Wu, K.J., Hryckowian, A.J., Bouley, D.M., Weimer, B.C., and Sonnenburg, J.L. (2014). Gut microbiota-produced succinate promotes C. difficile infection after antibiotic treatment or motility disturbance. Cell Host Microbe *16*, 770–777.

Ghorbani, M., Claus, T.H., and Himms-Hagen, J. (1997). Hypertrophy of brown adipocytes in brown and white adipose tissues and reversal of diet-induced obesity in rats treated with a beta3-adrenoceptor agonist. Biochem. Pharmacol. *54*, 121–131.

Grivennikov, S.I., Wang, K., Mucida, D., Stewart, C.A., Schnabl, B., Jauch, D., Taniguchi, K., Yu, G.Y., Osterreicher, C.H., Hung, K.E., et al. (2012). Adenoma-linked barrier defects and microbial products drive IL-23/IL-17-mediated tumour growth. Nature *491*, 254–258.

Guerra, C., Koza, R.A., Yamashita, H., Walsh, K., and Kozak, L.P. (1998). Emergence of brown adipocytes in white fat in mice is under genetic control. Effects on body weight and adiposity. J. Clin. Invest. *102*, 412–420.

Guerra, C., Navarro, P., Valverde, A.M., Arribas, M., Brüning, J., Kozak, L.P., Kahn, C.R., and Benito, M. (2001). Brown adipose tissue-specific insulin receptor knockout shows diabetic phenotype without insulin resistance. J. Clin. Invest. *108*, 1205–1213.

Hausmann, M. (2010). How bacteria-induced apoptosis of intestinal epithelial cells contributes to mucosal inflammation. Int. J. Inflamm. *2010*, 574568.

Kelly, C.P. (2013). Fecal microbiota transplantation–an old therapy comes of age. N. Engl. J. Med. *368*, 474–475.

Khoruts, A. (2014). Faecal microbiota transplantation in 2013: developing human gut microbiota as a class of therapeutics. Nat. Rev. Gastroenterol. Hepatol. *11*, 79–80.

Kopecky, J., Clarke, G., Enerbäck, S., Spiegelman, B., and Kozak, L.P. (1995). Expression of the mitochondrial uncoupling protein gene from the aP2 gene promoter prevents genetic obesity. J. Clin. Invest. *96*, 2914–2923.

Koren, O., Goodrich, J.K., Cullender, T.C., Spor, A., Laitinen, K., Bäckhed, H.K., Gonzalez, A., Werner, J.J., Angenent, L.T., Knight, R., et al. (2012). Host remodeling of the gut microbiome and metabolic changes during pregnancy. Cell *150*, 470–480.

Ley, R.E., Turnbaugh, P.J., Klein, S., and Gordon, J.I. (2006). Microbial ecology: human gut microbes associated with obesity. Nature *444*, 1022–1023.

Liou, A.P., Paziuk, M., Luevano, J.M., Jr., Machineni, S., Turnbaugh, P.J., and Kaplan, L.M. (2013). Conserved shifts in the gut microbiota due to gastric bypass reduce host weight and adiposity. Sci. Transl. Med. *5*, 178ra41.

Lowell, B.B., S-Susulic, V., Hamann, A., Lawitts, J.A., Himms-Hagen, J., Boyer, B.B., Kozak, L.P., and Flier, J.S. (1993). Development of obesity in transgenic mice after genetic ablation of brown adipose tissue. Nature *366*, 740–742.

Murphy, K.G., and Bloom, S.R. (2006). Gut hormones and the regulation of energy homeostasis. Nature *444*, 854–859.

Obermeier, F., Hausmann, M., Kellermeier, S., Kiessling, S., Strauch, U.G., Duitman, E., Bulfone-Paus, S., Herfarth, H., Bock, J., Dunger, N., et al. (2006). IL-15 protects intestinal epithelial cells. Eur. J. Immunol. *36*, 2691–2699.

Pelletier, M., Ratthé, C., and Girard, D. (2002). Mechanisms involved in interleukin-15-induced suppression of human neutrophil apoptosis: role of the anti-apoptotic Mcl-1 protein and several kinases including Janus kinase-2, p38 mitogen-activated protein kinase and extracellular signal-regulated kinases-1/2. FEBS Lett. *532*, 164–170.

Preidis, G.A., Ajami, N.J., Wong, M.C., Bessard, B.C., Conner, M.E., and Petrosino, J.F. (2015). Composition and function of the undernourished neonatal mouse intestinal microbiome. J. Nutr. Biochem. *26*, 1050–1057.

Ridaura, V.K., Faith, J.J., Rey, F.E., Cheng, J., Duncan, A.E., Kau, A.L., Griffin, N.W., Lombard, V., Henrissat, B., Bain, J.R., et al. (2013). Gut microbiota from twins discordant for obesity modulate metabolism in mice. Science *341*, 1241214.

Sato, T., Vries, R.G., Snippert, H.J., van de Wetering, M., Barker, N., Stange, D.E., van Es, J.H., Abo, A., Kujala, P., Peters, P.J., and Clevers, H. (2009). Single Lgr5 stem cells build crypt-villus structures in vitro without a mesenchymal niche. Nature *459*, 262–265.

Sekirov, I., Russell, S.L., Antunes, L.C., and Finlay, B.B. (2010). Gut microbiota in health and disease. Physiol. Rev. *90*, 859–904.

Sommer, F., and Bäckhed, F. (2013). The gut microbiota–masters of host development and physiology. Nat. Rev. Microbiol. *11*, 227–238.

Spehlmann, M.E., and Eckmann, L. (2009). Nuclear factor-kappa B in intestinal protection and destruction. Curr. Opin. Gastroenterol. *25*, 92–99.

Turnbaugh, P.J., Ley, R.E., Mahowald, M.A., Magrini, V., Mardis, E.R., and Gordon, J.I. (2006). An obesity-associated gut microbiome with increased capacity for energy harvest. Nature *444*, 1027–1031.

Wichmann, A., Allahyar, A., Greiner, T.U., Plovier, H., Lundén, G.O., Larsson, T., Drucker, D.J., Delzenne, N.M., Cani, P.D., and Bäckhed, F. (2013). Microbial modulation of energy availability in the colon regulates intestinal transit. Cell Host Microbe *14*, 582–590.

Wu, J., Boström, P., Sparks, L.M., Ye, L., Choi, J.H., Giang, A.H., Khandekar, M., Virtanen, K.A., Nuutila, P., Schaart, G., et al. (2012). Beige adipocytes are a distinct type of thermogenic fat cell in mouse and human. Cell *150*, 366–376.

Wu, J., Cohen, P., and Spiegelman, B.M. (2013). Adaptive thermogenesis in adipocytes: is beige the new brown? Genes Dev. *27*, 234–250.

Young, P., Arch, J.R., and Ashwell, M. (1984). Brown adipose tissue in the parametrial fat pad of the mouse. FEBS Lett. *167*, 10–14.